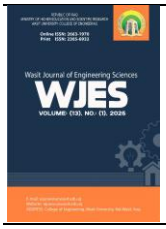

Wasit Journal of Engineering Sciences
Journal homepage: https://ejuow.uowasit.edu.iq

ISSN 2305-6932
Original Research

Vol. 14 No. 2 June 2026, pp.307-319
https://doi.org/10.31185/ejuow.v14i2.870

Effective Connectivity Patterns During Bilateral and Mirror-Induced Unilateral Hand Movements: An EEG Source-Level Study

Salim Mohammed Hussein Al-Wasity

Department of Electrical Engineering – College of Engineering – University of Wasit

Corresponding Author Email: salim@uowasit.edu.iq

Received Jan.8, 2026 | Revised Feb.25, 2026 | Accepted Mar.5, 2026 | Online Jun.1, 2026

ABSTRACT

This study aims to compare the effective connectivity patterns underlying two visuomotor processing tasks: bilateral hand movement and unilateral hand movement with mirror-box visual feedback. Electroencephalography and electromyography data were recorded using 44 and 2 electrodes respectively from 20 healthy participants while they performed the two tasks. Data were first preprocessed through epoching, band-pass filtering (1- 45Hz), artifact rejection, Independent Component Analysis, and source localization. Then a connectivity pattern estimators known as direct Directed Transfer Function were utilized to calculate the directed information flow amongst brain signal sources. The results identified distinct task- and frequency-dependent effective connectivity across visual, parietal, and sensorimotor regions. Such that, Beta-band coupling dominated during bilateral hand movements, while alpha-band connectivity decreased during mirror-box tasks. These findings support that source-localized Electroencephalography connectivity analyses can provide direct insights to investigate dynamic neural interaction and to guide and monitor rehabilitation therapies

Keywords: EEG, EMG, Effective Connectivity, Mirror-Box, Visuomotor Task

1. Introduction

Neuroimaging technology has advanced our understanding of the brain over the past decades due to the advances in both acquisition and analysis approaches. These approaches provide valuable insights into the functional organization of the human brain during variety of cognitive and behavioral tasks. Among them, Electroencephalography (EEG) is known for its high temporal resolution in millisecond allowing recording rapid signal oscillatory interactions across brain regions and networks. In particular, analyses of brain connectivity foster our understanding of how brain regions link and communicate with each other, offering innovative contributions to fundamental and clinical neuroscience [1].

Over the past three decades, brain connectivity analyses have been widely studied through diverse neuroimaging modalities and computational methods to better understand the neural mechanisms underlying cognition and rehabilitation. These computational methods include: structural connectivity analyses, driven by diffusion Magnetic Resonance Imaging (dMRI), map white matter tracts that connect cortical and subcortical regions [2], as well as, functional connectivity analyses, employed with functional MRI (fMRI), examine signals synchrony between distant brain regions during cognitive tasks, leveraging fMRI's high spatial resolution. However, fMRI temporal resolution (0.5-5 seconds) limits its ability to capture rapid neural dynamics or infer the directionality of information flow [3]. This temporal gap has motivated the use of EEG for connectivity analyses, as EEG provides millisecond temporal precision, facilitating the study of functional connectivity, statistical interdependence between neural signals, and effective connectivity, directed, causal influences among neural signals or regions [1][4].

In the context of motor-related research, accumulating evidence have identified the importance of beta-band (13- 30 Hz) oscillations for sensorimotor integration, movement preparation and execution [5]. Regarding mirror therapy, pioneered by Ramachandran for phantom limb pain [6], early fMRI work by Matthys et al. [7]

demonstrated that mirror illusion activates a network of visuomotor regions, including the premotor and parietal, and visual association regions. Subsequent EEG studies, such as that by Egsgaard et al., further showed altered cortical oscillation, particularly in alpha and beta power, during the mirror illusion [8]. Recently, Kim et al. utilized EEG-based dynamic causal modeling to reveal distinct connectivity signature between motor imagery and motor execution [9]. While Cheng et al. used magnetoencephalography to show that mirror feedback alters sensorimotor connectivity within the alpha-band [10]. However, the neural mechanisms underlying mirror-induced visuomotor processing remain insufficiently understood, particularly the directed, source-level, causal interactions between motor execution and mirror- guided unilateral movement.

To address this gap, this study examined the effective connectivity during two visuomotor tasks: bilateral hand movement and unilateral hand movement with a mirror-box using source-level EEG data of healthy participants. By applying the direct Directed Transfer Function (dDTF08) to Independent Component Analysis (ICA)-cleaned, source-localized EEG data, we identified the frequency-specific, directed interactions between somatosensory, parietal, and visual cortices with high temporal precision. This work makes three primary contributions to understanding the visuomotor integration through EEG-derived brain connectivity analysis. First, we employed the dDTF08 method to source-localized EEG data, rather than on sensor-level signals, to accurately map the dynamic causal organization of visuomotor networks and identify directed cortical information flows between somatosensory, visual and parietal cortices. Secondly, we directly compared, within the same cohort of healthy participants, two distinct visuomotor tasks to isolate the neural signature of mirror-box illusion which provides a reference for future clinical applications, particularly in neuroplasticity during mirror therapy interventions for phantom limb pain and post-stroke rehabilitation. Finally, our results demonstrate task- and frequency-specific connectivity patterns, including enhanced beta-band (13-30 Hz) coupling during bilateral hand task, and reduced alpha-band (8-13 Hz) coherence during mirror-box task, underscoring distinct neural mechanisms underlying these two visuomotor tasks.

2. Methods

2.1. Participants

Twenty healthy participants (mean age = 30.7 ± 2.3, female = 9), right-handed as assessed by the Edinburgh Handedness Inventory [11], participated in this experiment. All participants had normal or corrected-to-normal vision, no history of neurological disorders, psychiatric conditions, or upper limb impairments. The University of Glasgow ethics committee approved the protocol of the study, and all participants provided written informed consent prior to data collection.

2.2. Experimental Design and Tasks

Participants were instructed to perform two visuomotor tasks while seated. Each task consisted of eight sessions that lasted 108 seconds, with brief rest periods between sessions to prevent fatigue. Each session consisted of ten 2-second movement blocks alternating with eleven 8-second rest blocks.

2.2.1. Bilateral Hand Movement Task

Participants performed brisk, simultaneous bilateral hand and wrist flexion movements, self-paced at about 10-second intervals, with direct visual feedback of both hands placed naturally on the table as shown in Figure 1-A.

2.2.2. Unilateral hand movement with a mirror-box

For the mirror-box task, it is typically positioned in the sagittal plane between the patient's intact limb and the perceived phantom (hidden) limb as shown in Figure 1-B, to reflect the intact limb and perceive the reflection as the contralateral missing limb [7]. This reflection generates a perceptuo-motor conflict when the patient’s intact limb moves, creating a sensorimotor mismatch between visual feedback, tactile expectations, and proprioceptive signals [8].

In this task, participants performed identical brisk hand and wrist flexion movement by only the dominant right hand, while the left hand remained fully stationary behind a mirror-box. Participants were instructed to maintain visual attention on the reflected mirrored hand and avoid muscle activation in the hidden hand as shown in Figure 2.

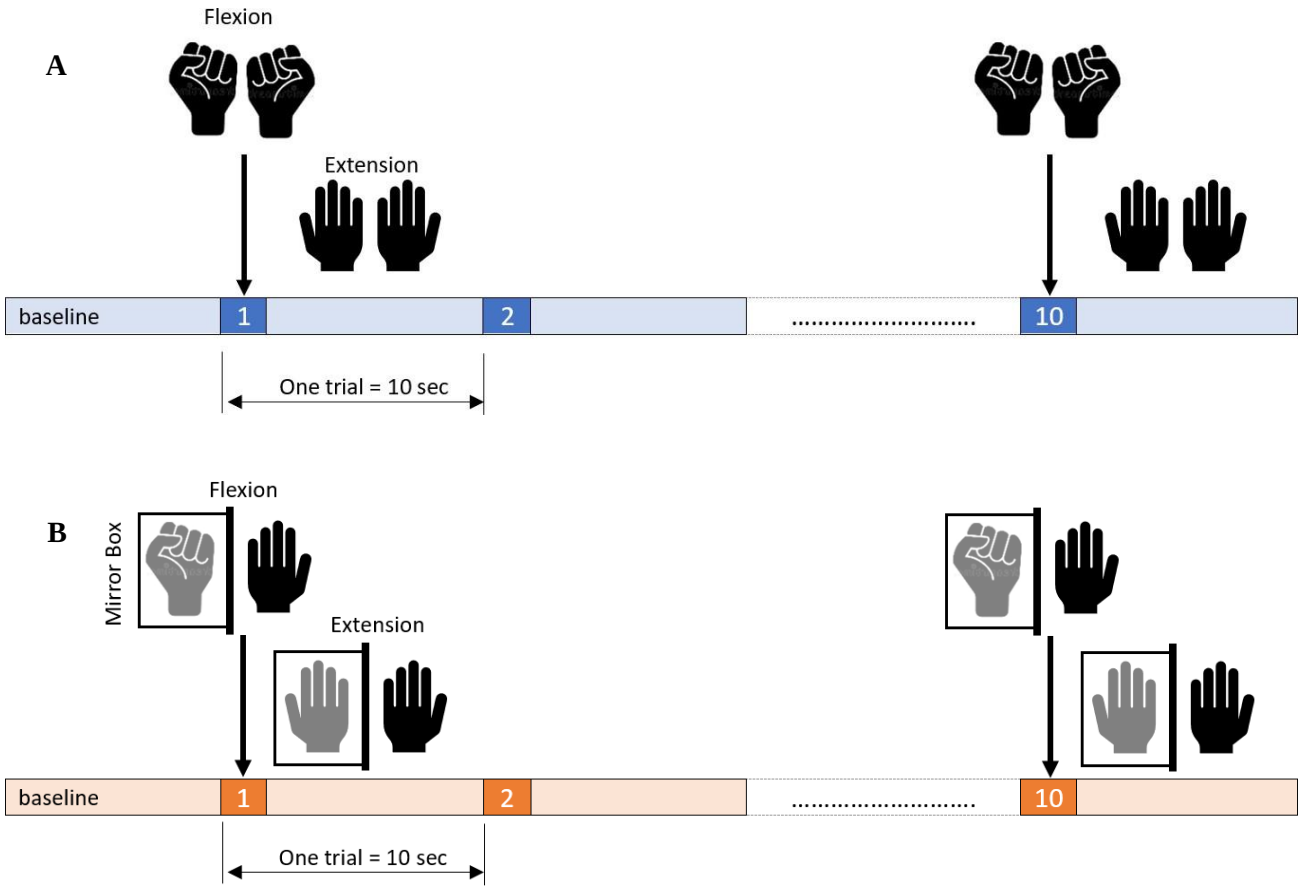

Figure 1. (A) Bilateral hand movement paradigm of one session. The session lasted for 108 seconds and consisted of ten 2 seconds bilateral movements blocks alternating with eleven 8 seconds rest blocks. (B) Unilateral Hand Movement with mirror-box paradigm of one session, lasted for 108 seconds and consisted of ten 2 seconds bilateral movements blocks alternating with eleven 8 seconds rest blocks.

Figure 2. The mirror-box apparatus, invented by Ramachandran for the study of phantom limb pain [6].

2.3. EEG and EMG Data Acquisition

2.3.1. Recording Setup

The recording setup comprised forty-four unipolar EEG channels and two bipolar EMG channels, amplified through three serially connected universal biosignal amplifiers (USBAmp, g.tec, Austria), with separate ground and reference electrodes. The amplifiers were configured with a 1.2 kHz sampling frequency, a 50Hz notch filter and band-pass filters (for EEG channels 1 - 100 Hz and for EMG channels 1 - 500Hz).

2.3.2. Electrode Configuration

EEG electrodes were placed according to the international 10-20 system [12]. Electrode locations are determined by dividing the head's circumference into 10% and 20% segments. Three other electrodes are placed laterally between standard landmarks in each hemisphere as shown in Figure 3. To achieve better scalp contact and reduce impedance (< 5 kΩ), a special conductive gel is applied between an EEG electrode and the scalp. The

EEG signals were initially recorded with a common reference electrode positioned at the ear lobule [13]. The EMG electrodes were adhered over both forearm flexor muscles to capture the onset and duration of hand and wrist flexion movements.

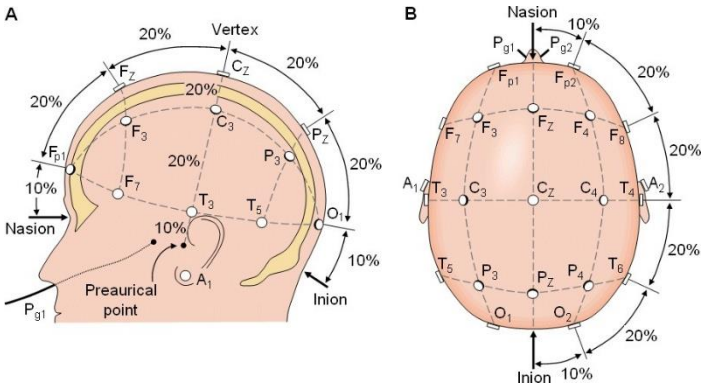

Figure 3. Schematic diagram of the international 10-20 electrodes location system for EEG signal recording, (A) sagittal view, (B) Axial view.

2.4. Data Preprocessing

Raw EEG data were preprocessed using EEGLAB (version 2014 Rio) [14], an open-source MATLAB toolbox (The MathWorks, Inc.). The preprocessing pipeline consisted of the following steps as shown in Figure 4.

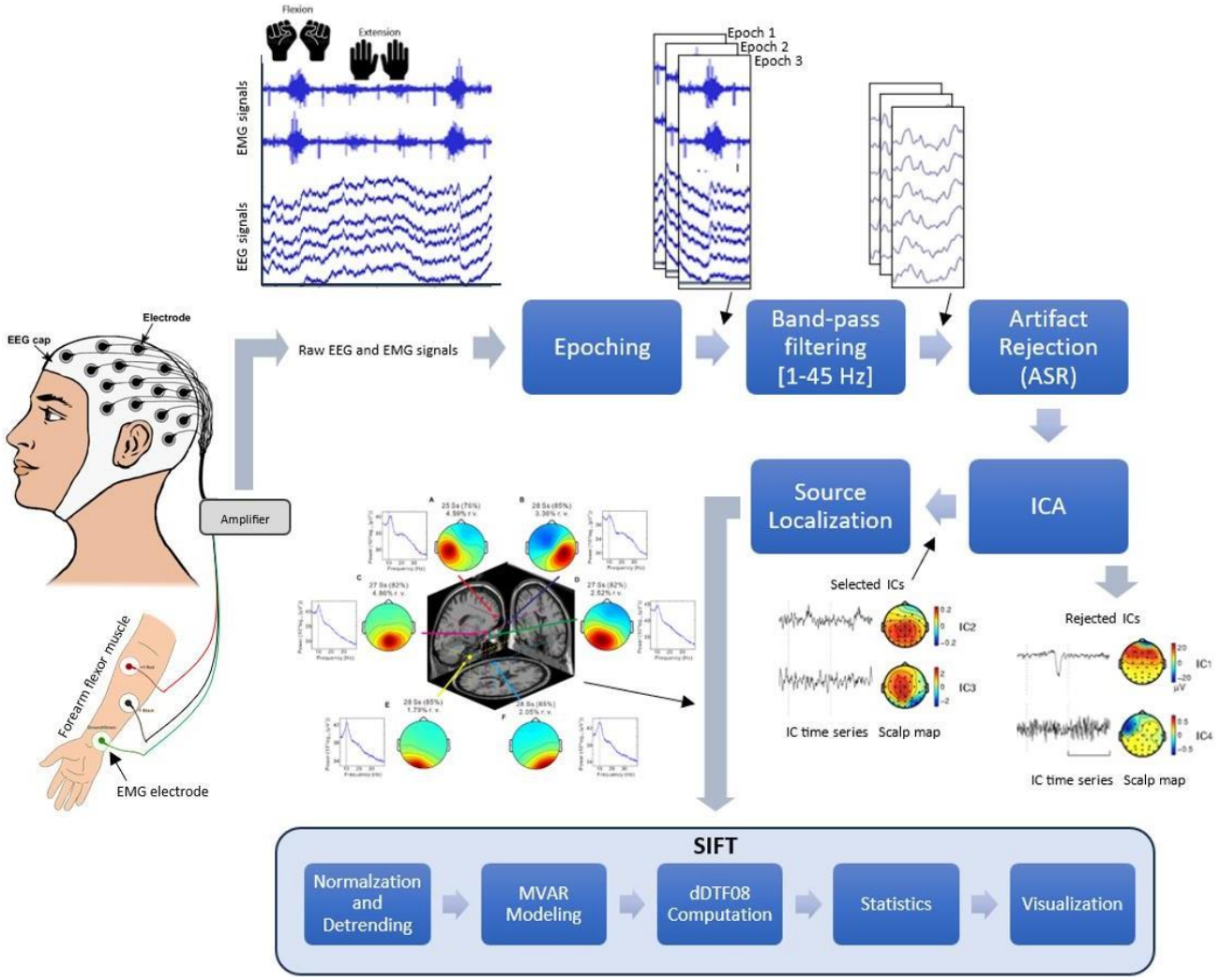

Figure 4. Schematic diagram illustrates the preprocessing and analysis pipeline of the EEG signal using EEGLAB and SIFT.

2.4.1. Artifact Rejection

Artifact-contaminated EEG channels were identified and removed based on abnormal statistics such as high variance and kurtosis threshold, and visual inspection of ocular (blinks, saccades), muscular (jaw clenching, neck tension), equipment related (environmental electromagnetic interference) and physiological (cardiac activity) artifacts [15]. These missing channels were replaced by interpolated clean data from the neighboring channels using the Artifact Subspace Reconstruction (ASR) plugin [16]. Finally, an ICA was applied as a blind source separation approach, using extended Infomax algorithm [14], to separate the neural signals from residual artifacts by decomposing the multichannel recorded EEG signal into statistically independent source signal. Mathematically, each observed signal $x_j(t)$ is modeled as a linear combination of n independent components (ICs) $s_i(t)$:

$$x_j(t) = a_{j1}s_1(t) + a_{j2}s_2(t) + \cdots + a_{jn}s_n(t) \quad (1)$$

Here, each mixture x_j and each source s_i are represented as random variables. Rewriting in vector-matrix form yields the mixing equation:

$$X = AS \quad (2)$$

Where X is the recorded EEG signal, A is the mixing weights a_{ji}, and S is the estimated source signal. Therefore, the ICs can be estimated by:

$$S = WX \quad (3)$$

where $W = A^{-1}$ is the unmixing matrix. Subsequently, ICs were characterized by their spatial scalp map, and time series. Artifactual components were visually inspected and removed using the Multiple Artifact Rejection Algorithm (MARA) plugin [17].

2.4.2. Source Localization

Equivalent dipoles, modeled as single sources or symmetric bilateral pairs, were estimated for each remaining IC using the DIPFIT plugin and manually refined to minimize residual variance between the IC scalp map and the forward model projection [18]. Mathematically, dipole parameters $\theta=\{r, q\}$, represent dipole position r and moment q, were estimated by minimizing

$$\min_{r,q} \|a_{IC} - L(r)q\|^2 \quad (4)$$

Where a_{IC} is the IC scalp map and $L(r)$ is the leadfield matrix at position r. ICs with residual variance above 15% or extracranial dipole locations were excluded. Finally, the remaining clean IC epochs, which are localized in sensorimotor, visual association, parietal, and prefrontal regions, were divided into two subsets corresponding to the two experimental tasks.

2.5. Effective Connectivity Analysis

Connectivity analysis was performed using the Source Information Flow Toolbox (SIFT) version 1.6 [18][19]. SIFT is an open-source EEGLAB-integrated toolbox, that provides a comprehensive pipeline for multivariate autoregressive (MVAR) modeling and causality analysis through five processing modules:

2.5.1. Data Preprocessing

The time series of the selected IC source signals were first normalized and linearly detrended to remove slow non-stationarities and DC offsets, improving MVPA model parameter estimation and accuracy.

2.5.2. MVAR Modeling

Multivariate autoregressive (MVAR) models of order p were fit to capture temporal dependencies among the multichannel IC source signals according to:

$$s(t) = \sum_{k=1}^{p} A_k s(t-k) + e(t) \quad (5)$$

Where *s(t)* is a vector of source signals at time *t*, *p* is the model order, A_k are coefficient matrices at lag *k* and *e(t)* is the residual noise vector. The optimal model order *p* was selected using Akaike (AIC) and Bayesian information criteria (BIC), which balance model fit and its complexity.

2.5.3. dDTF08 Computation

The effective connectivity between brain source signals was estimated using dDTF08, as implemented in SIFT toolbox. First, the MVAR model was transformed into the frequency domain using Fourier transformation, yielding the transfer function *H* defines as:

$$H(f) = \left(I - \sum_{k=1}^{p} A_k e^{\frac{-j2\pi f k}{f_s}} \right)^{-1} \quad (6)$$

Where *H(f)* is the frequency-domain transfer function at frequency *f*, *I* represent an identity matrix, *f* is frequency of interest (Hz), f_s is the sampling frequency (Hz). Then, the Directed Transfer Function (DTF) from source *j* to source *i* at frequency *f* was calculated as:

$$DTF_{i \leftarrow j}(f) = \frac{|H_{ij}(f)|}{\sqrt{\sum_{k=1}^{N} |H_{jk}(f)|^2}} \quad (7)$$

Where H_{ij} denotes the (*i*,*j*) element of the transfer function at frequency *f* that represents the influence of source *j* on source *i*, *N* is the total number of channels/ sources, and the denominator is a normalization factor that represents the total influence on source *i*. Finally, the dDTF08 was computed the product of the DTF and the partial coherence $P_{ij}(f)$, which suppresses indirect pathways by other sources [20] as follows:

$$dDTF08_{i \leftarrow j}(f) = DTF_{i \leftarrow j}(f) \times P_{i \leftarrow j}(f) \quad (8)$$

Where the partial coherence $P_{ij}(f)$ between source *j* and source *i* at frequency *f* is defined by:

$$P_{i \leftarrow j} = \frac{|S_{i \leftarrow j}(f)|^2}{S_{i \leftarrow i}(f) S_{j \leftarrow j}(f)} \quad (9)$$

Where $S_{ij}(f)$ denotes the cross-spectral density between sources *i* and *j*, and $S_{ii}(f)$ and $S_{jj}(f)$ represent the auto-spectral densities of sources *i* and *j*, respectively.

2.5.4. Statistical analysis

Statistical significance of the connectivity measures was evaluated using non-parametric bootstrap resampling [21]. Connections were considered statistically significant if their observed dDTF08 values exceeded the 95th percentile of the bootstrap distribution ($p < 0.05$, one-tailed test), corrected for multiple comparison using False Discovery Rate (FDR).

3. Results

3.1. ICA selection and localization

After preprocessing the EEG signal, including filtering, artifact rejection, and ICA decomposition, 13 ICs were selected per participant for further connectivity analyses. These ICs were localized across key cortical regions associated with visuomotor processing and control, spanning sensorimotor, visual association, parietal, and prefrontal cortices. Table 1 summarized the anatomical coordinates, and Brodmann Areas (BA) of the selected 13 ICs. The estimated dipole locations for all the ICs are shown in Figure 6, where:

- ICs in sensorimotor regions (BA 3, 5, 6, and 7) were localized in the percental and postcentral gyri, and were associated with motor preparation, coordination and execution.
- ICs in parietal regions (BA 40) were localized in the supramarginal gyrus and were responsible for visuomotor processing.

- IC in visual association region (BA 19) were localized in the occipital region, involved in mirror-box visual feedback.

3.2. Effective Connectivity analysis

The time-frequency dDTF08 spectrograms were generated using SIFT visualization tool, and they display directed information flow from -4 seconds to +3 seconds relative to movement onset (x-axis) across the 1-45 Hz frequency range (y-axis).

Table 1. Anatomical coordinates and corresponding BAs of the selected 13 ICs. RH and LH refer to the right and left hemisphere

IC No.	Coordinates (X, Y, Z)	BA	Hemisphere	Anatomical Name
1	20, -41, 72	5	RH	Superior Parietal Lobule (anterior part)
2	51, -55, 30	40	RH	Supramarginal Gyrus
3	38, -49, 64	7	RH	Superior Parietal Lobule (posterior part)
4	-38, -84, 30	19	LH	Extrastriate Visual Cortex (V3/V5 complex)
5	61, -16, 57	3	RH	Postcentral Gyrus (primary somatosensory cortex)
6	9, -49, 72	7	RH	Precuneus (medial superior parietal cortex)
7	15, -62, 67	7	RH	Precuneus (dorsal posterior section)
8	-66, -40, 23	40	LH	Supramarginal Gyrus
9	47, -1, 61	6	RH	Precentral Gyrus (premotor cortex - dorsal)
10	-58, 19, 34	9	LH	Middle Frontal Gyrus (dorsolateral prefrontal cortex)
11	47, 8, 54	6	RH	Precentral Gyrus (premotor cortex - ventral)
12	-9, -22, 72	6	LH	Supplementary Motor Area (SMA)
13	50, 1, 56	6	RH	Precentral Gyrus (premotor cortex - dorsal/ventral junction)

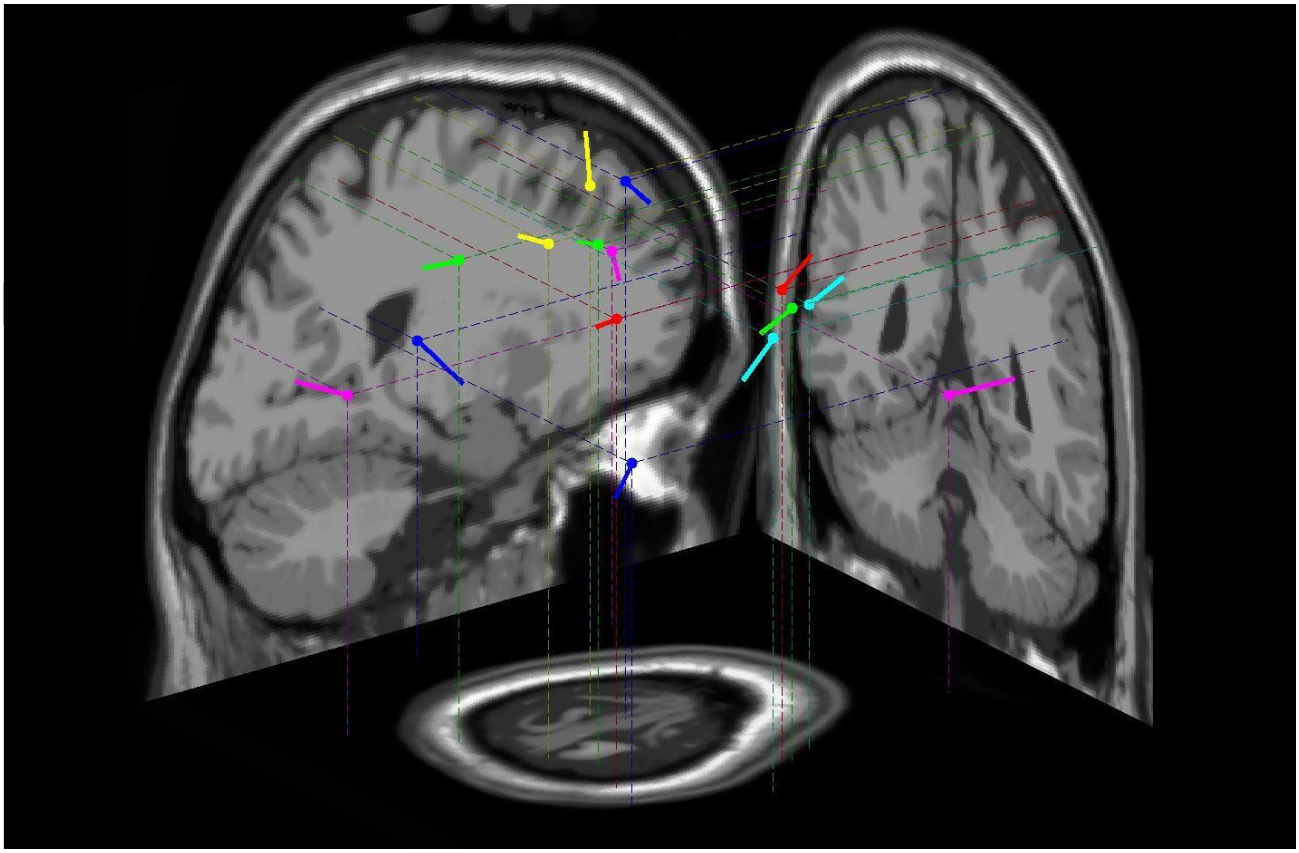

Figure 5. The spatial localization of the 13 source-localized ICs (dipoles) projected onto a standard brain template from sagittal, axial, and coronal views.

3.2.1. Effective Connectivity During Bilateral Hand Movement

The Time-frequency analysis of dDTF08 revealed three distinct patterns of directed information flow during the bilateral hand movement:

- **Visual-to-Parietal Information Flow (BA19 ↔ BA40)**

A significant connectivity ($p < 0.05$, FDR corrected) was observed between the left extrastriate visual cortex (IC4, BA19) to the right supramarginal gyrus (IC2, BA40) as shown in Figure 6. The upper panel illustrates strong feedforward dDTF08 flow from IC4 to IC2 within the beta-band spanning from -0.5s to +1s relative to movement onset, while the lower panel shows delayed and attenuated feedback from IC2 to IC4, at 0.2-0.3s after movement onset.

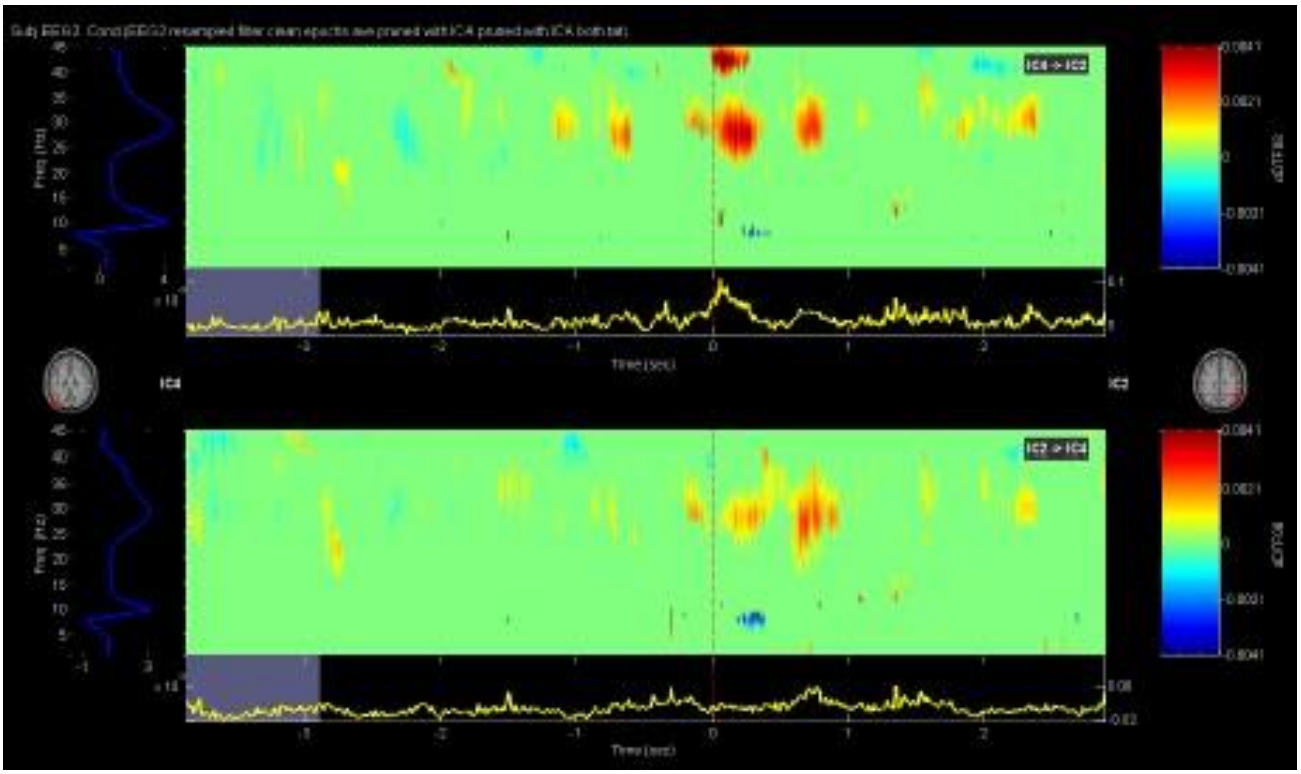

Figure 6. Time-frequency spectrograms of effective connectivity between IC4 (BA19, extrastriate visual cortex V3/V5) and IC2 (BA40, supramarginal gyrus) during bilateral hand movement. Upper panel: Feedforward connectivity (IC4→IC2) showing strong beta-band around movement onset (time = 0). Lower panel: Feedback connectivity (IC2→IC4) showing delayed, weaker beta-band coupling. x-axis displays time (-4 to +3 seconds) relative to movement onset (time = 0, marked by a red dotted vertical line), y- axis represents frequency band (1-45Hz), and Color scale represents the changes in dDTF08 connectivity relative to baseline. Red indicates increased information flow, blue indicates suppressed information flow, and green indicates no change.

- **Parietal-to-Visual Flow (BA7 → BA19)**

Figure 7, upper panel, displays a unidirectional information flow from right precuneus (IC7, BA7) to left extrastriate visual cortex (IC4, BA19) within the beta-band spanning from -1s to +1s relative to movement onset.

- **Within-Parietal Connectivity (BA7 ↔ BA7)**

In contrast to cross-regional pathways, connectivity between the right superior parietal lobule (IC3, BA7) and the precuneus (IC6, BA7) demonstrates distinct connectivity patterns. Figure 8, displays a bidirectional reduction in the feedforward and feedback alpha-band connectivity (10 Hz).

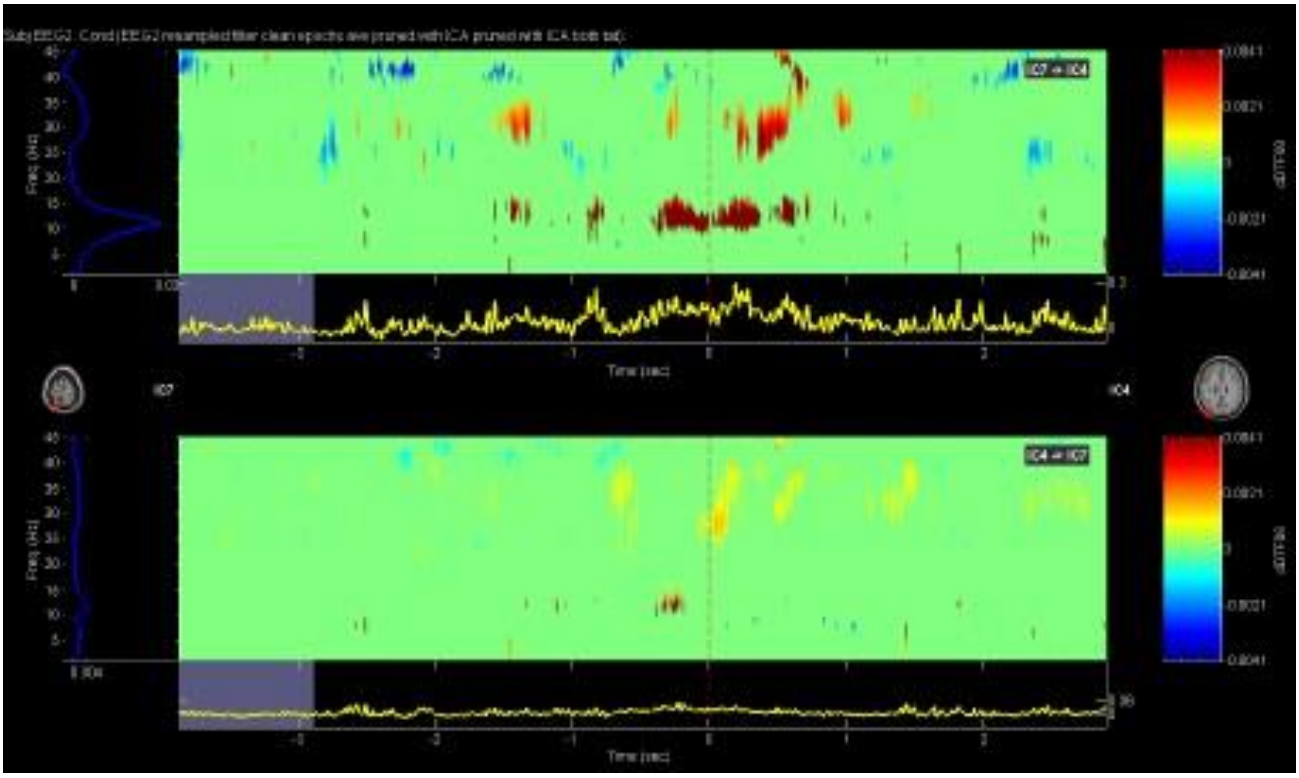

Figure 7. Time-frequency spectrograms of effective connectivity between IC7 (BA7, precuneus) and IC4 (BA19, extrastriate visual cortex) during bilateral hand movement. Upper panel: Feedforward connectivity (IC7→IC4) showing strong beta-band around movement onset. Lower panel: Feedback connectivity (IC4→IC7) showing no significant feedback coupling.

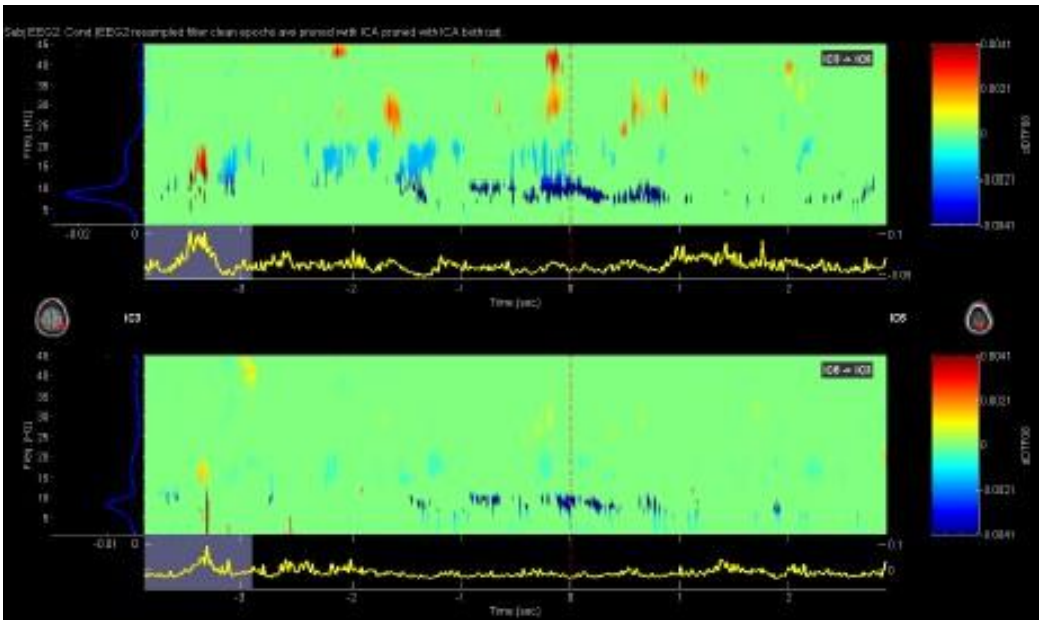

Figure 8. Time-frequency spectrograms of effective connectivity between IC3 (BA7, right superior parietal lobule) and IC6 (BA7, precuneus) during bilateral hand movement. Upper panel: Feedforward connectivity (IC3→IC6) showing a reduction in alpha-band (10 Hz) around movement onset. Lower panel: Feedback connectivity (IC6→IC3) showing attenuated feedback coupling in alpha-band.

3.2.2. Effective Connectivity During Unilateral Hand Movement with Mirror-box

The Time-frequency analysis of dDTF08 revealed distinct patterns of bidirectional information flow, during the unilateral hand movement with mirror-box, within the parietal regions. Figure 9 reveals the time-frequency

pattern between right superior parietal lobule (IC1, BA5) and right supramarginal gyrus (IC2, BA40). The upper panel shows a feedforward connectivity between IC1 to IC2, mainly suppression of alpha-band coupling (8-13HZ) after the movement onset and enhancing in the beta-band connectivity (13-25Hz) spanning from -1s to +1s relative to movement onset. The lower panel illustrates a similar delayed feedback connectivity between IC2 to IC1 in both alpha-band and beta-band, emerging at 0.2s to 1s post movement and at movement onset respectively. Similarly, the connectivity pattern between the right superior parietal lobule (IC3, BA7) and the precuneus (IC6, BA7) exhibit similar patterns during movement execution as shown in Figure 10. Strong reduction in the alpha-band connectivity persisted throughout the movement onset (-0.2 to 1.5s) with weaker improvement in beta-band around the movement onset.

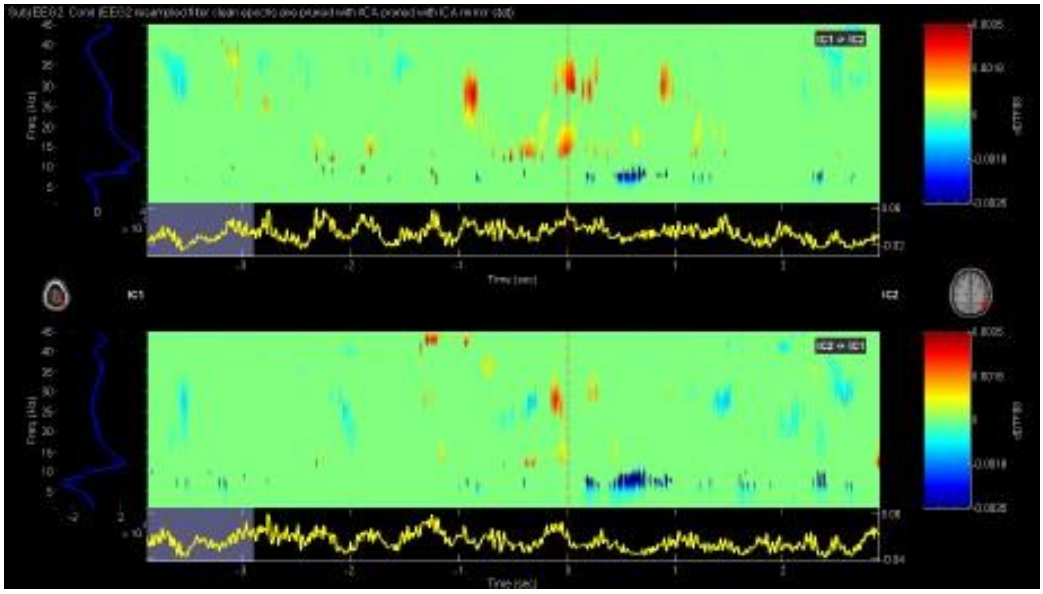

Figure 9. Time-frequency spectrograms of effective connectivity between IC1 (BA5, right superior parietal lobule) and IC2 (BA40, right supramarginal gyrus) during unilateral hand movement with mirror-box. Upper panel: Feedforward connectivity (IC1→IC2) showing a reduction in alpha-band (10 Hz) after the movement onset and enhancing in beta-band connectivity spanning -1s to +1 relative to the movement onset. Lower panel: Feedback connectivity (IC2→IC1) showing feedback coupling in alpha-band and beta-band.

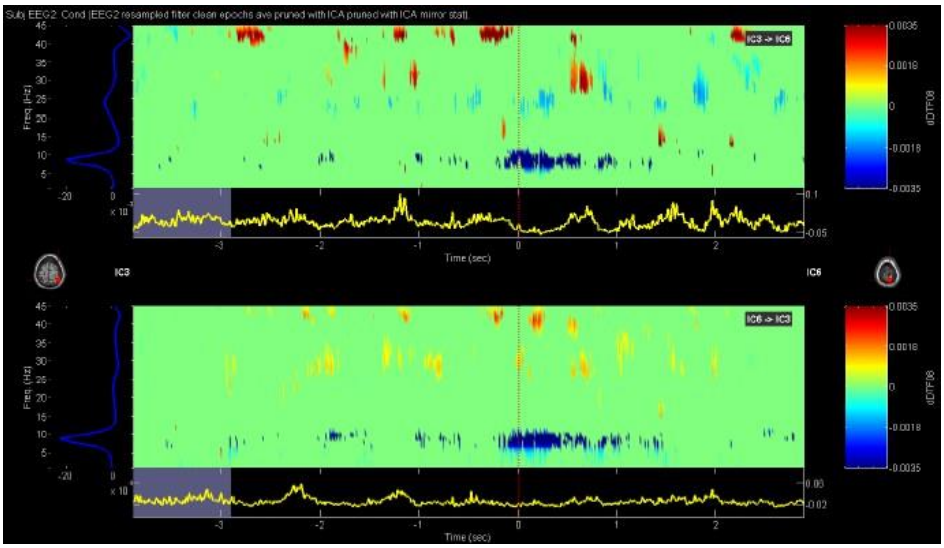

Figure 10. Time-frequency spectrograms of effective connectivity between IC3 (BA7, right superior parietal lobule) and IC6 (BA7, precuneus) during unilateral hand movement with mirror-box. Upper panel: Feedforward connectivity (IC3→IC6) showing a reduction in alpha-band (10 Hz) before and after the movement onset and enhancing in beta-band connectivity spanning -2s to +1 relative to the movement onset. Lower panel: Feedback connectivity (IC6→IC3) showing feedback coupling in alpha-band and beta-band.

4. Discussion

In this study, we examined and compared the effective connectivity patterns during two visuomotor tasks: bilateral hand movements and unilateral hand movements with mirror-box visual feedback using dDTF08 analysis applied on source-localized EEG signal. Our results identified distinct tasks- and frequency-specific directed information flow between visual, parietal, and sensorimotor regions, such that bilateral hand movements engaged predominantly beta-band coupling across parietal-occipital regions, whereas mirror visual feedback elicited by alpha-band suppression in parietal region.

During bilateral hand movement task, our results showed a dominant directed information flow in beta-band (13-30 Hz) between visual and parietal regions, supporting the role of real-time visual feedback in coordinating bilateral hand coordination. In particular, we observed a strong feedforward beta-band coupling, with minimal feedback, between extrastriate visual cortex (V3/V5), which is involved in processing visual motion, and the supramarginal gyrus, a central hub for multisensory integration and visuomotor coordination. This connectivity pattern, strong feedforward with weak feedback, aligns with predictive coding frameworks [4]. In this context, during bilateral movements with congruent visual feedback, visual regions send predictive signals about expected sensory trajectories of movement to sensorimotor areas, while feedback connections, which convey prediction errors, would be minimal when the expectations are met. Critically, our observation of feedforward beta coupling is supported by Barone and Rossiter who suggest that such beta synchrony is essential for predictive coding, where the brain down-weights sensory errors when the movement outcome matches the internal model, as seen in our reliable bilateral task [22]. Moreover, the reciprocal beta-band coupling between the extrastriate visual cortex and the precuneus, which is responsible for coordination of bilateral movements and visuospatial imagery, indicates continuous visuospatial integration [23]. In contrast to these cross-regional interactions, connectivity within the parietal regions, specifically between superior parietal lobule, involves sensory integration and motor planning, and precuneus shows a bidirectional reduction in alpha-band information flow, reflecting the active involvement of parietal regions in spatial planning of the self-paced hand movements. These findings align with the recent EEG studies in understanding sensorimotor integration through effective connectivity analyses. For example, Wang et al. found that beta-band coherence is associated with motor recovery following stroke, highlighting its role in how the brain reorganizes after injury [24]. A very recent work by [25] showed that even motor imagery recruits beta-mediated pathways between motor and posterior parietal-occipital regions, highlighting how beta rhythm supports visuomotor integration and spatial attention in visual processing networks. The dominant beta-band connectivity we observed in parietal-occipital regions complements existing evidence, confirming that visual motion processing is essential for guiding bilateral coordination and maintaining stable sensorimotor control.

By contrast, mirror-box task engaged visuospatial and mirror-system networks, reflected by distinct bidirectional connectivity patterns in alpha-band (8–12 Hz) desynchronization centered on the parietal cortices. Notably, we observed a feedforward reduction in alpha-band combined with an enhancement in beta-band between the superior parietal lobule and the supramarginal gyrus resulted from a perceptuo-motor conflict between visual input, that suggest bilateral movement, and proprioceptive and tactile signal, that confirm only unilateral movement. This conflict appeared as delayed and attenuated feedback connectivity around 300-500ms post movement onset, indicating disrupted sensory reafference, where the expected sensory feedback follows motor commands. Additionally, we observed similar alpha-band connectivity profile between superior parietal lobule and the precuneus, suggesting that the recruitment of distinct neural mechanisms to inhibit the conflict sensory information from the moving reflected hand and the stationary hidden hand [1]. The suppression of alpha-band connectivity observed during mirror-box tasks extends previous findings on the neural mechanisms of mirror therapy by providing novel insights into directed connections that earlier research could not cover. For instance, Ding et al. found that mirror visual feedback in a hand task triggered significant bilateral alpha-band network changes, reflecting mirror neuron system activation [26]. Another recent work by Bonnal et al. demonstrated strong alpha event-related desynchronization in central-parietal regions during lower-limb visual feedback therapy, attributing this to mirror system involvement [27]. These studies support our observation that mirror tasks induce alpha-band suppression within parietal regions, which reflect the "unblocking" of parietal cortex inhibition pathways to allow the processing of illusory visual feedback, and overriding the conflicting proprioceptive signal from the stationary hand.

Overall, our findings have important clinical and rehabilitative applications, for example, beta-band directed connectivity may serve as a biomarker for motor recovery. As a result, it provides a framework for guiding

personalized rehabilitation protocols for patients with sensorimotor impairments. However, several limitations must be addressed. First, the sample size was limited to 20 healthy participants, which may limit the generalizability of these findings to clinical cohorts. Secondly, the current study did not examine the sustained effective connectivity during prolonged effect of mirror exposure or the long-term neuroplastic effects following mirror therapy sessions. Future longitudinal clinical trials will be essential to validate these connectivity biomarkers as reliable predictors of motor recovery.

5. Conclusion

In summary, this study explored and compared the effective connectivity pattern during bilateral hand movement and unilateral hand movement with a mirror-box visual feedback using source-localized EEG analysis. Bilateral movement task enhanced beta-band information flow between visual and parietal networks, consistent with the top-down predictive coding framework during congruent visuomotor integration. In contrast, the mirror-box task suppressed alpha-band directed connectivity within parietal network, reflecting the cognitive control mechanisms for resolving perceptuo-motor conflict. These findings highlight the potential of source-localized EEG effective connectivity analysis to monitor neural reorganization and to guide rehabilitation interventions of sensorimotor patients. To translate these insights into clinical practice, future works should employ larger clinical cohorts, and longitudinal designs to validate these findings and improve reproducibility.

Declaration of Competing Interest

The authors declare that there are no conflicts of interest regarding the publication of this manuscript.

Funding Information

No funding was received from any financial organization to conduct this research

References

[1] P. M. Rossini, M. A. N. Ferilli, L. Rossini, and F. Ferreri, “Clinical neurophysiology of brain plasticity in aging brain,” Curr. Pharm. Des., vol. 19, no. 36, pp. 6426–6439, 2013.
[2] E. Bullmore and O. Sporns, “Complex brain networks: Graph theoretical analysis of structural and functional systems,” Nat. Rev. Neurosci., vol. 10, no. 3, pp. 186–198, 2009.
[3] G. Deshpande, S. LaConte, G. A. James, S. Peltier, and X. Hu, “Multivariate Granger causality analysis of fMRI data,” Hum. Brain Mapp., vol. 30, no. 4, pp. 1361–1373, 2009.
[4] K. J. Friston, “Functional and effective connectivity: A review,” Brain Connect., vol. 1, no. 1, pp. 13–36, 2011.
[5] L. Pollonini et al., “Information communication networks in severe traumatic brain injury,” Brain Topogr., vol. 23, no. 2, pp. 221–226, 2010.
[6] V. S. Ramachandran and E. L. Altschuler, “The use of visual feedback, in particular mirror visual feedback, in restoring brain function,” Brain, vol. 132, no. 7, pp. 1693–1710, 2009
[7] K. Matthys, S. Smits, A. Van der Geest, R. Van der Lugt, E. Seurinck, and S. Swinnen, “Mirror-induced visual illusion of hand movements,” Arch. Phys. Med. Rehabil., vol. 90, no. 4, pp. 675–681, 2009.
[8] L. L. Egsgaard, L. Petrini, G. Christoffersen, and L. Arendt-Nielsen, “Cortical responses to the mirror-box illusion: A high-resolution EEG study,” Exp. Brain Res., vol. 215, no. 3–4, pp. 345–357, 2011.
[9] Y. K. Kim, E. Park, A. Lee, C. H. Im, and Y. H. Kim, “Changes in network connectivity during motor imagery and execution,” PLoS ONE, vol. 13, no. 1, 2018.
[10] C. H. Cheng, S. H. Lin, C. Y. Wu, Y. H. Liao, K. C. Chang, and Y. W. Hsieh, “Mirror illusion modulates M1 activities and functional connectivity patterns of perceptual–attention circuits during bimanual movements: A magnetoencephalography study,” Front. Neurosci., vol. 13, Art. 1363, 2019.
[11] R. C. Oldfield, “The assessment and analysis of handedness: The Edinburgh inventory,” Neuropsychologia, vol. 9, no. 1, pp. 97–113, 1971.
[12] M. Teplan, “Fundamentals of EEG measurement,” Meas. Sci. Rev., vol. 2, no. 2, pp. 1–11, 2002.
[13] W. J. Freeman, “Imaging brain function with EEG,” in Imaging Brain Function with EEG, C. M. Michel and D. Brandeis, Eds. New York, NY, USA: Springer, 2013, pp. 87–123.

[14] A. Delorme and S. Makeig, “EEGLAB: An open source toolbox for analysis of single-trial EEG dynamics including independent component analysis,” J. Neurosci. Methods, vol. 134, no. 1, pp. 9–21, 2004.
[15] W. O. Tatum, B. A. Dworetzky, W. D. Freeman, and D. L. Schomer, “Artifact: Recording EEG in special care units,” J. Clin. Neurophysiol., vol. 28, no. 3, pp. 264–277, 2011.
[16] T. R. Mullen, N. Bigdely-Shamlo, C. Kothe, K. Gramann, and S. Makeig, “Real-time modeling and 3-D visualization of source dynamics and connectivity using wearable EEG,” in Proc. Annu. Int. Conf. IEEE EMBS, Osaka, Japan, 2013, pp. 2184–2187.
[17] I. Winkler, S. Haufe, and M. Tangermann, “Automatic classification of artifactual ICA-components for artifact removal in EEG signals,” Behav. Brain Funct., vol. 7, no. 1, Art. no. 30, 2011.
[18] A. Delorme, T. Mullen, C. Kothe, Z. A. Acar, N. Bigdely-Shamlo, A. Vankov, and S. Makeig, “EEGLAB, SIFT, NFT, BCILAB, and ERICA: New tools for advanced EEG processing,” Comput. Intell. Neurosci., vol. 2011, Article ID 130714, 2011.
[19] T. R. Mullen, A. Delorme, C. Kothe, and S. Makeig, “An electrophysiological information flow toolbox for EEGLAB,” Biol. Cybern., 2010.
[20] S. L. Bressler, C. G. Richter, Y. Chen, and M. Ding, “Cortical functional network organization from autoregressive modeling of local field potential oscillations,” Stat. Med., vol. 26, no. 21, pp. 3875–3885, 2007.
[21] B. Efron and R. J. Tibshirani, An Introduction to the Bootstrap. New York, NY, USA: Chapman & Hall, 1993.
[22] J. Barone and H. E. Rossiter, “Understanding the role of sensorimotor beta oscillations,” Front. Syst. Neurosci., vol. 15, Art. 655886, May 2021
[23] G. Plomp, C. Quairiaux, C. M. Michel, and L. Astolfi, “The physiological plausibility of time-varying Granger-causal modeling,” NeuroImage, vol. 97, pp. 206–216, 2014.
[24] C. Wang, X. Yang, D. Guo, W. Huo, N. Yu, and Y. Zhang, “Transcranial direct current stimulation–induced changes in motor cortical connectivity are associated with motor gains following ischemic stroke,” Sci. Rep., vol. 14, Article 15645, 2024
[25] H. Zhou and K. Iramina, “Discovery of EEG effective connectivity during visual motor imagery with multi-scale symbolic transfer entropy,” Sci. Rep., 2025.
[26] Q. Ding, T. Lin, G. Cai, Z. Ou, S. Yao, H. Zhu, and Y. Lan, “Individual differences in beta-band oscillations predict motor-inhibitory control,” Front. Neurosci., vol. 17, Article ID 1138406, 2023.
[27] A. Adham, B. T. Le, J. Bonnal, H. Bessaguet, E. Ojardias, P. Giraux, P. Auzou, “Neural basis of lower-limb visual feedback therapy: An EEG study in healthy subjects,” J. Neuroeng. Rehabil., vol. 21, Art. 114, 2024